A priori error-based mesh adaptation in CFD

Eléonore Gauci, Anca Belme, Alexandre Carabias, Adrien Loseille, Frédéric Alauzet, Alain Dervieux

1 Introduction

The main purpose of Computational Mechanics research is not to obtain more efficient computational methods on existing cases (or more accurate, which is somewhat equivalent). This purpose is to perform new computations which were not affordable before. Future researchers will hopefully be able to face the many challenges of the century (global change, health, energy). This remark holds (to a lesser extend) for mesh adaptation research. The purpose is to be able to compute new phenomena and also to master the numerical uncertainties which have been up to now unsufficiently controlled.

Many phenomena in continuum mechanics real world involve multiple scales or/and singularities and cannot be computed with uniform meshes. Designing non uniform meshes will become so complex that automatic adaptation will be mandatory.

Eléonore Gauci
Université Côte d'Azur, Inria, 2004 Route des lucioles, F-06902 Sophia-Antipolis, e-mail: Eleonore.Gauci@inria.fr

Anca Belme
Sorbonne Université, Université Paris 06, CNRS, UMR 719, Institut Jean le Rond d'Alembert Tours 55-65, Bureau 406, Case 162, 4 Place Jussieu, F-75452 Paris, e-mail: belme@dalembert.upmc.fr,

Alexandre Carabias
Société Lemma, 10 rue Melingue F-75019 Paris, e-mail: Alexandre.Carabias@lemma-ing.com,

Adrien Loseille · Frédéric Alauzet
INRIA Saclay Ile-de-France 1, rue Honor d'Estienne d'Orves F-91126 Palaiseau, e-mail: Adrien.Loseille@inria.fr, Frederic.Alauzet@inria.fr,

Alain Dervieux
Société Lemma, 2000 Route des lucioles, F-06410 Biot, and Inria, e-mail: alain.dervieux@inria.fr

Second-order accurate anisotropic mesh adaptation has demonstrated that phenomena which were impossible to compute with non-adaptive meshes become computable even on medium size computers. The first section of this paper shows an example. But adaptive or not second-order methods are limited to routine computation for a low accuracy, typically with a 1% relative error. In many cases this is sufficient for applications and coherent with the accuracy of available models (e.g. basic statistical turbulence modeling). When a smaller error tolerance $(0.1\%, 0.01\%)$ is necessary, second-order accurate methods become quite inefficient.
Also, second-order accurate methods are definitively inefficient for many unsteady phenomena (e.g. wave propagation or with instability) The error accumulates while time is advanced. Due to multiple scales, explicit time-stepping can be prohibitive. Implicit time-stepping deteriotates the fastest waves. Then higher-order adaptive methods must be developed in order to efficiently adress the accuracy question.

To sum up this first discussion, there is a class of computations which are not possible without an increase of *efficiency*. Efficiency generally results from accuracy, algorithmics, and computers. We concentrate here on the increase of accuracy of approximation through mesh adaptation.

Since we need to improve the efficiency of mesh adaptation, we need to have tools to measure and predict it, replacing human intuition and heuristics by mathematical concepts. The existing mathematical roadmap for error control is the result of many scientific contributions. A mathematical definition of the mesh adaptation purpose was proposed by the introduction of *goal-oriented* formulations [12] dealing with the accuracy in the evaluation of a prescribed scalar output. But reducing the error of solely a scalar output is not always sufficient for the engineer who wants to increase its understanding by looking at the computed flow, or wants to use it for building reduced order models. Thanks to *norm-oriented* formulations [13, 14], error control applies to solution fields and Banach norms. At the other end of the process, namely the mathematical definition of the control parameter, the replacement of the mesh by a Riemannian metric allowed for transforming the mesh adaptation issue into a well-posed optimization problem. Finally we have the optimal mesh (according to our preferences) and, at least for the norm-oriented option described in the sequel, we have an idea of the numerical error.

This paper presents a review of recent theoretical advances together with examples of applications. In particular the mesh adaptation roadmap which we define extends to higher-order accurate approximation and to unsteady phenomenas. This review is accompanied by new insights. Among others, we revisit the application of a mathematical analysis predicting the asymptotic accuracy of the higher-order adaptation algorithm when the solution field contains singularities.

2 Feature-, goal-, and norm-oriented formulations

The three formulations are presented for the second-order accurate particular case of P^1 approximations on triangles and tetrahedra.

2.1 Feature-based (FB) adaptation

The feature-based anisotropic mesh adaptation criterion is inspired by the classical finite-element *a priori* estimate. It assumes that a good mesh for the *interpolation* of the unknown (or of one or several sensors depending on it) is a good mesh for a Partial Differential Equation (PDE) approximation based on the same interpolation. This method is generally defined in a continuous framework by replacing the local interpolation error by the application of the Hessian of the exact solution times a local mesh size defined by a continuous metric, see [1, 2, 4, 5, 6, 7, 8]. It can be also defined on a discrete basis as in [28].

Given a numerical solution W_h, a solution of higher regularity $R_h(W_h)$ is *recovered*, so that the following interpolation error estimate [9, 11] holds:

$$\|R_h(W_h) - \Pi_h R_h(W_h)\|_{L^p} \leq N^{-\frac{2}{3}} \left(\int_\Omega \det\left(|H_{R_h(W_h)}|\right)^{\frac{p}{2p+3}} \right)^{\frac{2p+3}{3p}},$$

where $H_{R_h(W_h)}$ is the Hessian of the recovered solution and N an estimate of the desired number of nodes. Notation Π_h holds for the usual elementwise affine interpolation relying on values at vertices. When working in the continuous mesh framework [10, 11], we also have the optimal metric field leading to the previous error estimate:

$$\mathscr{M}_{\mathbf{L}^p} \;=\; \mathscr{K}_{L^1}\left(\left|H_{R_h(W_h)}\right|\right) \;=\; D_{\mathbf{L}^p}\left(\det\left|H_{R_h(W_h)}\right|\right)^{\frac{-1}{2p+3}} \left|H_{R_h(W_h)}\right|.$$

If anisotropic mesh prescription is naturally deduced in this context, interpolation-based methods do not take into account the features of the PDE. However, in some simplified context and assumptions (elliptic PDE, specific recovery operator R_h), we have:

$$\|W - W_h\| \leq \frac{1}{1-\alpha}\|R_h(W_h) - \Pi_h R_h(W_h)\| \quad \text{with } \; 0 \leq \alpha < 1,$$

so that a good convergence to the exact solution may be observed [15]. Indeed, if $R_h(W_h)$ is a better approximate of W in the following sense:

$$\|W - W_h\| \;\leq\; \frac{1}{1-\alpha}\|R_h(W_h) - W_h\| \quad \text{with } \; 0 \leq \alpha < 1,$$

and if the reconstruction operator R_h has the property:

$$\Pi_h R_h(W_h) = W_h,$$

then we can bound the approximation error of the solution by the interpolation error of the reconstructed function $R_h(W_h)$:

$$\|W - W_h\| \leq \frac{1}{1-\alpha}\|R_h(W_h) - \Pi_h R_h(W_h)\|.$$

Note that from a practical point of view, $R_h(W_h)$ is never recovered, only its first and second derivatives are estimated. Standard recovery techniques include least-square, L^2-projection, Green formula or the Zienkiewicz-Zhu recovery operator. For all the numerical examples, the $\mathbf{L}^2$ norm is used with the L^2-projection to recover derivatives.

These estimates are very efficient to capture anisotropic physical phenomenon. A typical example is the prediction of the sonic boom signature of a supersonic aircraft. Indeed, in the case, every singularities of the geometry generates a shock waves that propagates down to the ground. All physical variables (density, pressure, ...) are discontinuous accross the shock. Special features dedicated to sonic boom mesh adaptation are discussed in [2]. To illustrate the use of FB mesh adaptation, we consider the C25D geometry of the 2nd Sonic-Boom Prediction Workshop [32] represented in Figure 1. We use the Mach number as sensor. The sequence of generated meshes is reported in Table 1. Several cuts in the volume mesh and the imprint of the adapted mesh in the symmetry plane are depicted in Figure 2.

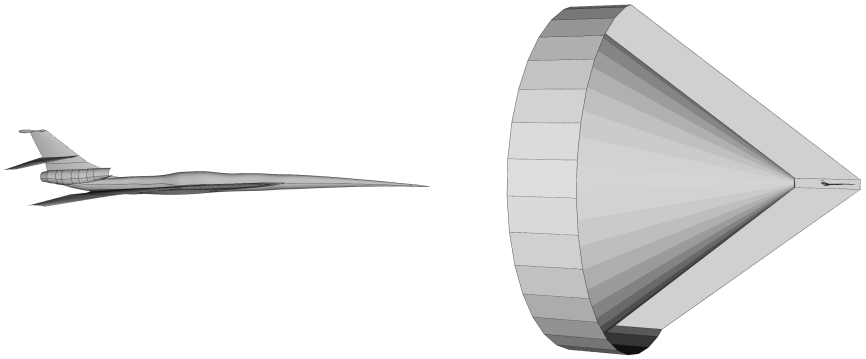

Fig. 1 Lowboom C25 Geometry (left) and typical computational domain, around this geometry, aligned with Mach cone, used for the "tailored mesh"(right).

# vertices	# tetrahedra	mean ratio	mean quotient
1 946 918	11 093 526	10	97
5 529 916	32 726 736	18	297
12 953 271	77 497 813	18	325
27 644 454	166 148 147	19	400

Table 1 Lowboom C25 example: Statistics for the sequence of adapted meshes. Ratio holds for the aspect ratio defined on any element as $max_i h_i / min_i h_i$. Quotient is defined on any element as $max_i h_i^3/(h_1 h_2 h_3)$ and measures the gain with respect to an isotropic mesh.

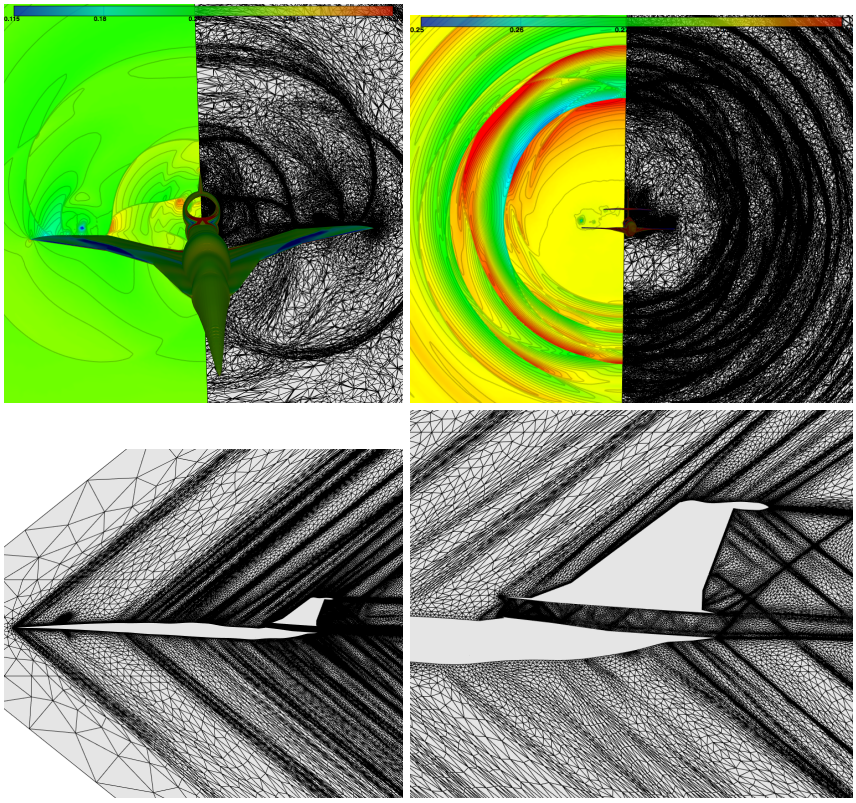

Fig. 2 Lowboom C25 example: Cut plane $x = 30$ (top left) and $x = 50$ (top right) and meshes on the symmetry plane (bottom left) and close view near the inlet (bottom right).

The feature-based approach is particularly attractive due to its simplicity and to the interest in taking into account physical aspects through the choice of the sensors. However, for systems, the choice of sensors is extremely sensitive. Some additional mathematics for defining the best choice, through the goal-oriented approach, are required for most complex applications.

2.2 The goal-oriented formulation

The goal-oriented (GO) mesh adaptation, as stated before, focuses on deriving the optimal mesh for computing a prescribed scalar quantity of interest (QoI). This method is *a priori* different from the optimal mesh for a field/state. It is particulary suitable for a large class of problems in computational mechanics where one wants to better understand/compute such a quantity of interest (e.g. drag, lift coef-

ficients, vorticity in a wake, a mass flow across a surface, etc,) while maintaining a reasonable cost. Such GO methods require however the computation of an adjoint state. Adjoint-based methods were known to be particulary useful in optimal control/design, where the computational cost for evaluating sensitivities can be importantly reduced using the adjoint-state. It has been also proved for a few years that using an adjoint is efficient for improving by a correction the accuracy of the evaluation of a quantity of interest ([17]). As GO mesh adaptation is concerned, a remarkable quantity of papers deals with *a posteriori* goal-based error formulation to drive adaptivity, using adjoint formulations or gradients (see for example [19, 18]). Our group is investigating GO formulations for steady and unsteady problems in an *a priori* context. Loseille *et al.* [14] derived the goal-based error estimate in a steady context for Euler flows, showing that the QoI error estimate is expressed as a weighted interpolation error on solution flow fields. This leads to an optimal metric computed as a sum of Hessians of Euler flux fields weighted by gradient components of the adjoint state.

A short description of our goal-based *a priori* error estimation for the compressible Navier-Stokes system is now presented.

For simplicity, the QoI j is assumed to be the scalar product of the state solution W by a given field g, $j(w) = (g,W)$ where W is the exact state solution to the continuous model $\Psi(W) = 0$. We denote by W_h the solution of a discretisation, $\Psi_h(W_h) = 0$. Let W^* be the adjoint state, satisfying $(\partial\Psi/\partial W)W^* = g$. Under adhoc regularity assumptions concerning Ψ, Ψ_h, W and W^*, we have ([14]) the following compact form for our *a priori* error estimate:

$$\begin{array}{l} |(\Psi(W) - \Psi_h(\Pi_h W), \Pi_h W^*)| \ \preceq \\ \qquad \int_\Omega \sum_k \ G_k(W, \nabla W^*, |\,\rho_H(W^*)|) \ \left|S_k(W) - \Pi_h S_k(W)\right| \mathrm{d}\Omega\,, \end{array} \tag{1}$$

where $A \preceq B$ holds for a majoration asymptotically valid, *i.e.* $A \leq B + o(A)$ when mesh size tends to zero. Expression $|\,\rho_H(\varphi)\,|$ holds for spectral radius of the Hessian of φ. The interest of such an estimate is that the error model is a sum of interpolation errors weighted by algebraic functions of state and adjoint.

Let us consider the example of the Navier-Stokes system:

$$\Psi(W) = 0 \text{ on } \Omega, \text{ with } \Psi(W) = \nabla\cdot\mathscr{F}^E(W) + \nabla\cdot\mathscr{F}^V(W) \tag{2}$$

where $W = {}^t(\rho, \rho\mathbf{u}, \rho E)$ is the conservative flow variables vector and vector $\mathscr{F}^E$ represents the Euler fluxes, and $\mathscr{F}^V$ the viscous fluxes defined hereafter:

$$\mathscr{F}^V(W) = [0, \sigma, -(\mathbf{q} - \mathbf{u}\cdot\sigma)]^T \quad ; \quad \sigma = \mu(\nabla\mathbf{u} + \nabla\mathbf{u}^{\mathrm{T}}) - \frac{2}{3}\mu\nabla\cdot\mathbf{u}\mathbf{I},$$

with μ representing the constant viscosity. The heat flux $\mathbf{q}$ is given by Fourier's law $\mathbf{q} = -\lambda\nabla T$, where λ is the heat conduction (assumed here to be constant). We have noted ρ the density, $\mathbf{u} = (u_1, u_2, u_3)$ the velocity vector, $H = E + p/\rho$ is the

total enthalpy, $E = T + \frac{\|\mathbf{u}\|^2}{2}$ the total energy and $p = (\gamma - 1)\rho T$ the pressure with $\gamma = 1.4$ the ratio of specific heat capacities, T the temperature, and $(\mathbf{e}_1, \mathbf{e}_2, \mathbf{e}_3)$ the canonical basis. Expliciting Formulation (1) for the Navier-Stokes equations leads to the following developement:

$$|(\Psi(W) - \Psi_h(\Pi_h W), \Pi_h W^*)| \preceq \mathscr{E}$$

with:

$$\begin{aligned}
\mathscr{E} = & \int_\Omega |\nabla W^*| \cdot \left| \mathscr{F}^E(W) - \Pi_h \mathscr{F}^E(W) \right| d\Omega \\
& + \left(d + \frac{1}{3} \right) K_d \sum_{i=1}^{d} \int_\Omega \mu \, |\rho_H(W^*_{\rho u_i})| \, |u_i - \Pi_h u_i| \, d\Omega \\
& + \frac{1}{3} K_d \sum_{i=1}^{d} \sum_{\substack{j=1 \\ j \neq i}}^{d} \int_\Omega \mu \, |\rho_H(W^*_{\rho u_i})| \, |u_j - \Pi_h u_j| \, d\Omega \\
& + K_d \int_\Omega \lambda \, |\rho_H(W^*_{\rho E})| \, |T - \Pi_h T| \, d\Omega \\
& + (d + \frac{1}{3}) K_d \sum_{i=1}^{d} \int_\Omega \mu \, |\rho_H(W^*_{\rho E})| \, |u_i| \, |u_i - \Pi_h u_i| \, d\Omega \\
& + \frac{1}{3} K_d \sum_{i=1}^{d} \sum_{\substack{j=1 \\ j \neq i}}^{d} \int_\Omega \mu \, |\rho_H(W^*_{\rho E})| \, |u_i| \, |u_j - \Pi_h u_j| \, d\Omega \\
& + \frac{5}{3} \sum_{i=1}^{d} \sum_{\substack{j=1 \\ j \neq i}}^{d} \int_\Omega \mu \left| \frac{\partial (\Pi_h W^*_{\rho E})}{\partial x_j} \left((u_j - \Pi_h u_j) \frac{\partial u_i}{\partial x_i} - (u_i - \Pi_h u_i) \frac{\partial u_j}{\partial x_i} \right) \right| d\Omega \,,
\end{aligned}$$

in which $K_d = 3$ in two dimensions, $K_d = 6$ in three dimensions. Taking into account *all* the terms in $\mathscr{E}$ is a sufficient condition for an efficient GO adaptation. These terms are computed only once for each mesh considered in the adaptation loop.

As illustration, we consider the 3D computation of a turbulent shock-boundary layer interaction problem. A similar problem was addressed with FB mesh adaptation in [3]. The shock is initiated by a diamond shape obstacle in side a rectangular channel. The zone of interest is the region where the shock hits the bottom of the channel. The incoming flow field is defined such that: $M_\infty = 1.4$, the angle of attack $\alpha = 0$ and $Re = 3.6 \times 10^6$. The QoI is the drag on the bottom flate plate. A mesh adaptation loop has been applied for a total number of vertices of 1.5 million.

The complex shock waves pattern is accurately captured by the adaptive process in all the regions where it impacts the flat plate. We observe that at the end of the domain, the mesh is rather coarse. In contrast, the boundary layer is highly refined. A close-up view of the shock boundary-layer interaction region shows that we cap-

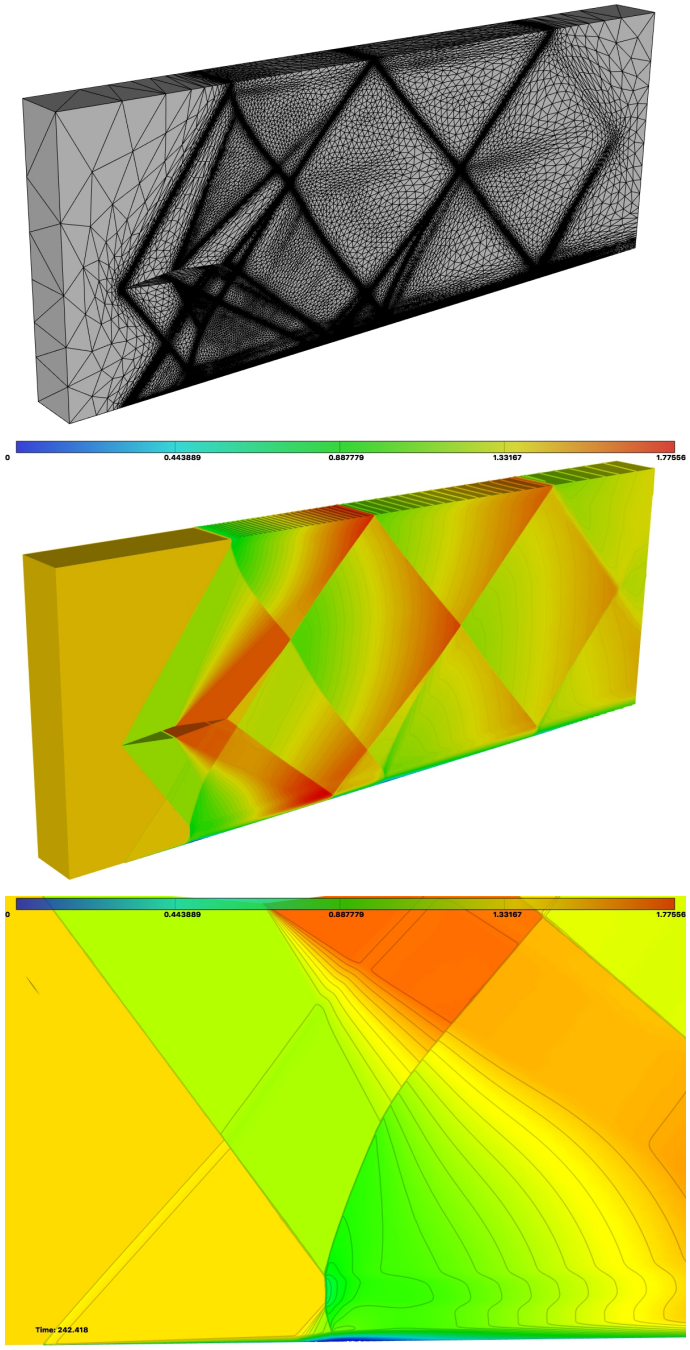

Fig. 3 Goal Oriented mesh adaptation of the viscous flow in a channel with diamond-shape obstacle. Global mesh (top), global pressure solution (middle) and zoom on the beginning and thickening of the bottom boundary layer (bottom).

ture accurately the separation bubble and the lift off of the boundary layer due to the impact of the oblique shock. We also capture the reflected shock in front of the bubble and the expansion fan at the foot of the oblique shock. All these waves are visible in the mesh.

Remark 1: During the presentation of this work at the conference, O. Pironneau raised some paradox in the proposed goal-oriented adaptation algorithm. The question was: how can you adequately adapt with a criterion expressed in terms of the state and adjoint state if you do not adapt for a *better state* and a *better adjoint*?

This question is related to a particular step in the design of the mesh adaptation algorithm. Indeed, the first step in our theory is to apply a *continuous* metric analysis, which produces a continuous optimality system involving continuous state, continuous adjoint and continuous stationarity with respect to the metric.

In a second step, we have to *discretize* the whole optimality system. For this, an option *could be* to use a sequence of uniformly refined meshes. State and adjoint would be well refined. This option would finally produce (with a prohibitive computational cost) the optimal metric.

Once we have a good approximation of the optimal metric, we can generate unit adapted meshes based on it. By construction, these meshes are adequate for the evaluation of the functional, through the evaluation of the state. In other words the state computed with an unit mesh of the metric is a good mesh for the functional evaluation. At the same time, with this adapted mesh, the state is not well computed since only its features influencing the functional are supposed to be well computed. Adapting for a better state would then be *not optimal*.

Adapting for a better adjoint is a somewhat *second-order* approach, since it does not influence directly the quality of the approximation of the functional, but solely how close is the metric from the perfectly optimal one : formally, an ε-large deviation of the (unconstrained) quasi-optimum provokes an ε^2-large deviation of the (smooth) functional value. A similar argument applies to an adaptation for the stationarity equation.□

Remark 2: The GO method (as explained here) shows the following limitations:
- It allows to minimize the error on a functional, but does not give an idea of the effective error on this functional, but the corrector of [17] can be used as an approximation of it.
- In many cases the engineer needs a good evaluation of the fields themselves.
The norm-oriented technology described in next section addresses these two issues.□

2.3 Numerical corrector

Given a discrete problem, a mesh (of metric) $\mathscr{M}_h$ and the discrete solution W_h computed with the mesh, we call "numerical corrector" a discrete field W_h' such that the sum $W_h + W_h'$ is a significantly more accurate approximation of the exact solution

than W_h. In other words, W'_h is a good approximation of the error. Clearly, W'_h is useful for estimating the error, for correcting it, and by the way for building the norm-oriented mesh adaptation algorithm defined in Section 2.4.

A trivial way to compute W'_h could be to first compute an extremely accurate and extremely costly $W_{h/2^k}$ (k large) solution computed on a mesh $\mathscr{M}_{h/2^k}$ obtained by dividing k times the elements of $\mathscr{M}_h$, and finally to put $W'_h = W_{h/2^k} - W_h$. But the interesting feature of a numerical corrector should be that its computational cost is *not much higher* than the computational cost of W_h. We describe now a corrector evaluation of low computational cost relying on the application of a Defect Correction principle and working on the initial mesh $\mathscr{M}_h$:

$$\Psi_h(W_h + \bar{W}'_{h,DC}) \approx -R_{h/2\to h}\Psi_{h/2}(R_{h\to h/2}W_h) \quad ; \quad W'_{h,DC} = \frac{4}{3}\bar{W}'_{h,DC} - (\pi_h W_h - W_h)$$

where the $\pi_h W_h - W_h$ is a recovery-based evaluation of the interpolation error (see [14] for details). The notation $R_{h/2\to h}$ holds for the transfer (extension by linear interpolation) operator from the twice finer mesh $\mathscr{M}_{h/2}$ to the initial mesh $\mathscr{M}_h$. The notation $R_{h\to h/2}$ holds for the transfer (restriction) operator from the the initial mesh $\mathscr{M}_h$ to the twice finer mesh $\mathscr{M}_{h/2}$. The finer-mesh residual $\Psi_{h/2}(W_h)$ can be assembled by defining the sub-elements of $\mathscr{M}_{h/2}$ only locally around any vertex of $\mathscr{M}_h$.

Applications of this method to the Navier-Stokes model can be found in [27]. We present an application with the Euler model used for sonic boom prediction. We consider again the C25 geometry. The important input is the pressure signature at one-body length below the aircraft.

Figures 4,5 depict the pressure signal and the local error bar, from the non linear corrector, for a sequence of tailored meshes (meshes aligned with the Mach cone, Figure1) and for adapted meshes. The pressure perturbation on axis ($z = 0$) concentrates between abscissa $x = 40$ and $x = 90$. Mesh convergence does not clearly hold after $x = 60$ for both series of calculations. This is probably explained by the extreme complexity of the many shocks interacting in this region, which are captured in details with the adapted meshes (see Figure2). Let us concentrate on the interval $40 < x < 60$. The left-side calculations seem converged as values are concerned but the corrector remains large. The right-side show a more coherent convergence, with a corrector also getting smaller.

2.4 The norm-oriented (NO) formulation

In order to obtain a good evaluation of a solution field, the user has to specify the field and also in which norm the approximated field should close to the exact one. Of course the choice of this norm is constrained by an admissibility statement: typically, a second-order accurate unstructured scheme will generally not provide a convergent prediction of the third-order derivative of the solution. Another important output of NO is an evaluation of the approximation error.

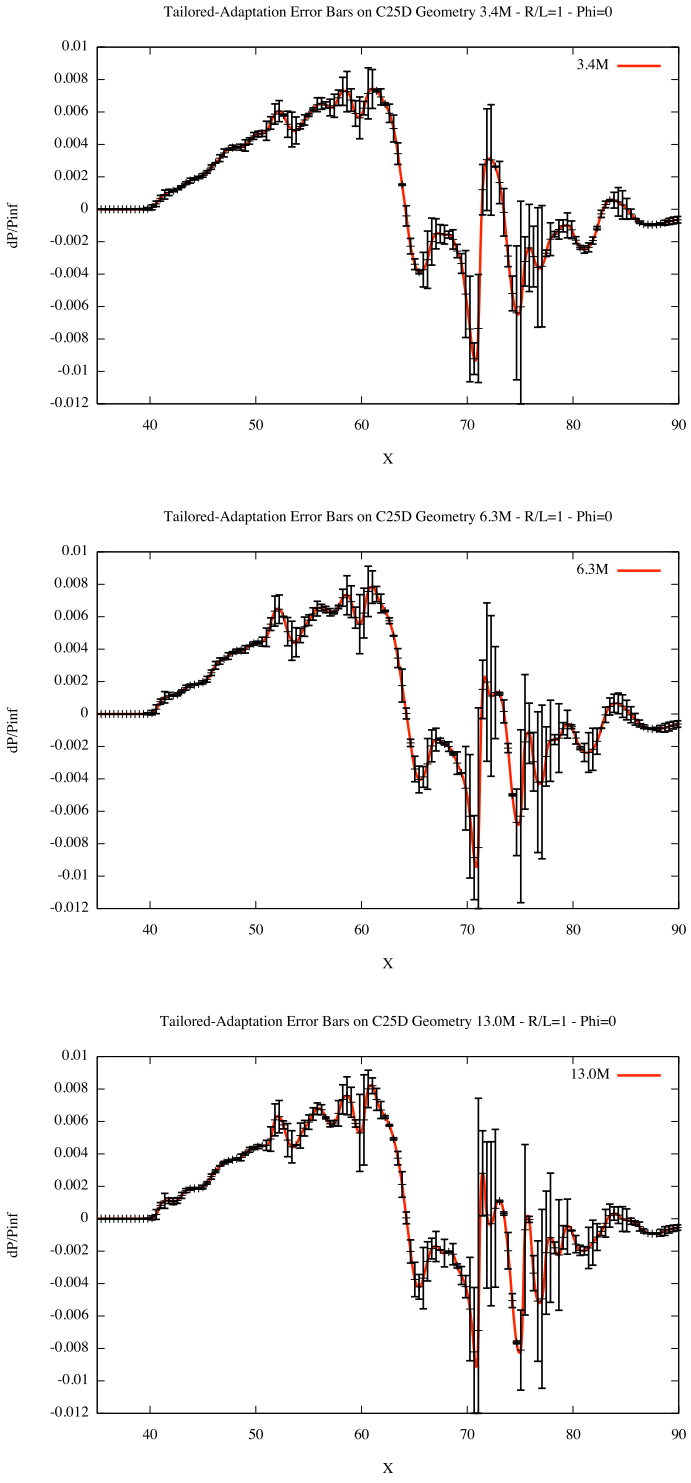

Fig. 4 Lowboom C25 example: Pressure levels (red) and non-linear corrector (black) predictions of the pressure on tailored meshes.

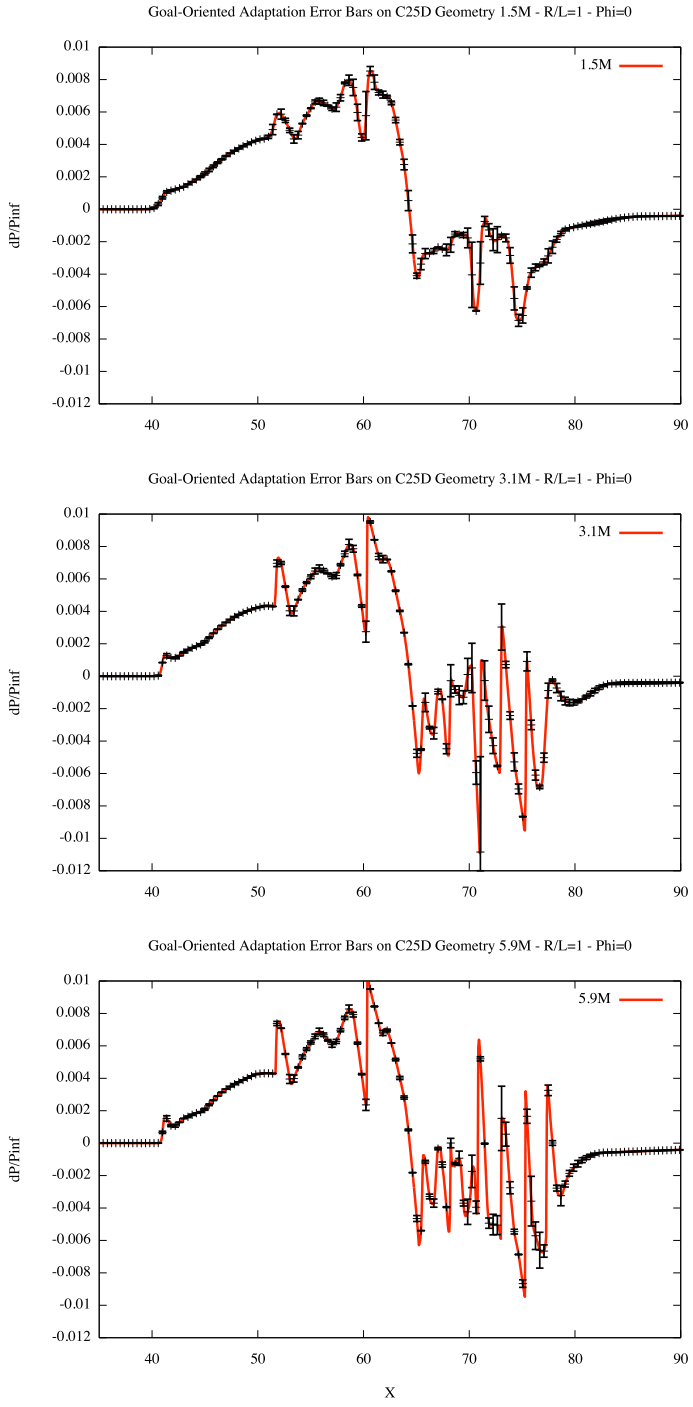

Fig. 5 Lowboom C25 example: Pressure levels (red) and non-linear corrector (black) predictions of the pressure on adapted goal-oriented meshes .

We describe now a norm-oriented approach relying on the L^2 norm. It consists in the minimization of the following expression with respect to the mesh $\mathscr{M}$:

$$j(\mathscr{M}) = ||W - W_{\mathscr{M}}||^2_{L^2(\Omega)}. \tag{3}$$

where the state $W_{\mathscr{M}}$ is solution of the discretised PDE on a unit mesh for $\mathscr{M}$:

$$\Psi_{\mathscr{M}}(W_{\mathscr{M}}) = 0 \tag{4}$$

Introducing $g = W - W_{\mathscr{M}}$, we get a formulation similar to a goal-oriented formulation:

$$j(\mathscr{M}) = (g, W - W_{\mathscr{M}}). \tag{5}$$

The central idea of NO is to replace g by a numerical corrector W'_h as defined in previous section. The rest of the NO process, follows the GO algorithm with $g = W'_h$. The whole NO adaptation algorithm finally writes:

Step 1: solve state equation
Step 2: solve corrector equation
Step 3: solve adjoint equation
Step 4: evaluate optimal metric
Step 5: generate unit mesh for $\mathscr{M}_{opt,norm}$ and go to *Step 1*.

In order to give an idea of how this NO works, we consider as *benchmark* a test case from [20] featuring a 2D boundary layer (Figure 6) for comparing a feature-oriented calculation with a norm-oriented one. The Laplace equation is solved with a RHS inducing the boundary layer depicted in the figure. When the feature-based method is applied, a tremendous improvement of the error is obtained with 128 vertices, then a uniform element division and a feature-oriented adaptation are applied in alternance. The L^2 error norm (ordinates) is measured from the analytic solution. While the element division is applied, the error is as expected divided by 4. In contrast, for 512, 2048,... vertices (abscissae), the effect of feature-oriented adaptation is to *increase* the error. This illustrates the fact that asymptotically the direction of a better interpolation deviates from the direction of a better approximation. As a consequence, with a feature-based adaptation, the second-order convergence can be lost. At the contrary, with this test case, each NO mesh-adaptation phase improves (even slightly) the error norm, producing an asymptotic numerical convergence of order two. When $30,000$ vertices are used, the error is more than two orders of magnitude lower than with the uniform refinement.

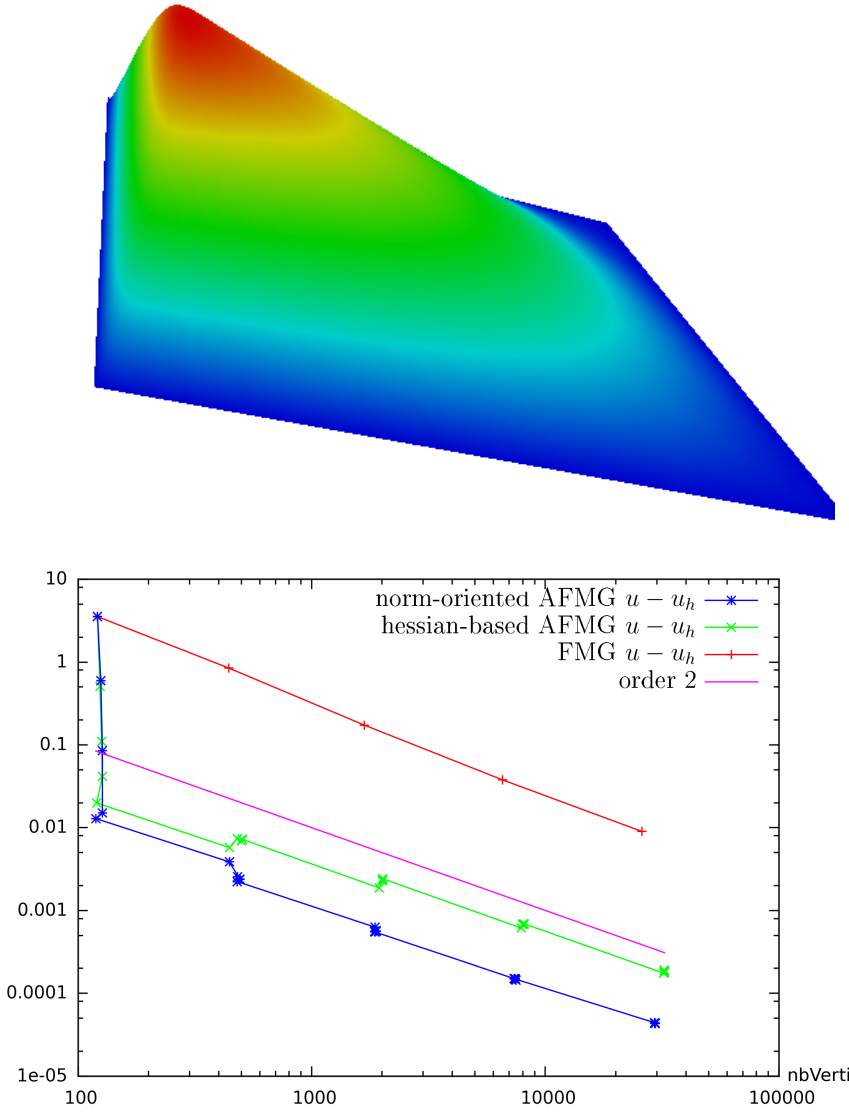

Fig. 6 Elliptic test case of a 2D boundary layer. A comparison between uniform refinement ("FMG"), feature/Hessian-based, and norm-oriented mesh adaptation methods: error $|u - u_h|_{L^2}$ in terms of number of vertices.

3 High-order and unsteady schemes

Due to their error size and characteristics (dispersion, dissipation), second-order accurate approximations are unable to compute many phenomena. For smooth contexts, high-order methods bring crucial improvements. But, as soon as singularities are involved in the model, they fail in producing a sufficient numerical convergence. Typical real life examples are sound propagation in media containing cracks, or flow with interfaces. Relative errors less than two-three orders of magnitude in continuous media with singularities is a challenge for computational mechanics. To address this challenge, high-order (HO) mesh adaptation methods extending to singular cases need be defined.

3.1 High-order estimates

Main existing HO schemes satisfy the so-called $k-$exactness property expressing the fact that if the exact solution is a polynomial of order k then the approximation scheme will give the exact solution as answer. Inside these schemes is involved a step of polynomial reconstruction (e.g. ENO schemes), or of polynomial interpolation (e.g. Continuous/discontinuous Galerkin). The main part of the error can then be expressed in terms of a $(k+1)$-th term of Taylor series where the spatial increment is related with local mesh size.

We want to stress that this is the key of an easy extension of metric-based adaptation to HO schemes. We illustrate this with the computation of 2D Euler flows. Considering a triangulation of the computational domain and its dual cells C_i built with triangle medians, the exact solution W of Euler equations verifies:

$$B(W,V_0)=0,\ \ \forall\ V_0\in\mathscr{V}_0=\{V_0\ \text{ constant by cell}\},$$

with (omitting initial conditions):

$$\begin{aligned} B(W,V_0) &= \int_0^T\left\{\sum_i E_j(W,V_0)\right\}dt+\int_0^T\int_{\partial\Gamma}\mathscr{F}_\Gamma(W)\cdot\mathbf{n}V_0 d\Gamma dt \\ E_j(W,V_0) &= \int_{C_i} v_0\frac{\partial\pi_0 W}{\partial t}d\Omega+\frac{1}{2}\int_{\partial C_i}V_0(\mathscr{F}(W)|_{\partial C_i}+\mathscr{F}(W)|_{\partial C_j})\cdot\mathbf{n}d\sigma \end{aligned}$$

where we denote by π_0 the operator replacing a function by its mean on each cell. Let us define a *quadratic Central-ENO scheme* [21, 22]. The computational cost of this scheme is rather large but acceptable for 2D calculations (its extension to 3D is even more computationally expansive). This scheme is based on a quadratic reconstruction on any integration cell C_i using the means of the variable on cells around C_i. Let us denote R_2^0 the global reconstruction operator mapping the constant-by-cell discrete field into its quadratic-by-cell reconstruction. The CENO scheme writes in short:

Find W_0 constant by cell s.t. $B(R_2^0 W_0, V_0) = 0, \ \forall \ V_0$ constant by cell.

A representative functional of goal-oriented error is:

$$\delta j = (g, R_2^0 \pi_0 W - R_2^0 W_0).$$

Lemma[23]: *Introducing the adjoint state $W_0^* \in \mathcal{V}_0$, solution of:*

$$\frac{\partial B}{\partial W}(R_2^0 W_0)(R_2^0 V_0, W_0^*) = (g, R_2^0 V_0), \ \forall \ V_0 \in \mathcal{V}_0. \tag{6}$$

we have the following equivalence:

$$(g, R_2^0 \pi_0 W - R_2^0 W_0) \approx \frac{\partial B}{\partial u}(W)(R_2^0 \pi_0 W - W, W_0^*) \quad \textit{as mesh size tends to zero.}\square$$

This estimate is typical of a k-exact variational scheme and permits to express the error δj as a Taylor term of rank $k+1$, rank 3 in our case, with respect to mesh size $\delta \mathbf{x}$:

$$\delta j \preceq \sup_{\delta \mathbf{x}} \mathbb{T} (\delta \mathbf{x})^3 \quad \text{as mesh size tends to zero.} \tag{7}$$

In [23] an equivalent pseudo-Hessian $\tilde{H}_i$ is evaluated by least squares

$$\sup_{\delta \mathbf{x}} \mathbb{T} (\delta \mathbf{x})^3 \cong \left(sup_{\delta \mathbf{x}} |\tilde{H}| (\delta \mathbf{x})^2 \right)^{\frac{3}{2}} \quad \forall \delta \mathbf{x} \in \mathbb{R}^2. \tag{8}$$

Then an optimal metric can be obtained in a similar way to the second-order accurate case. An *a priori* better option, not tested here, is proposed in [26].

3.2 High-order accurate unsteady mesh adaptation

We illustrate the use of the above estimate (7), (8) with an application to an unsteady flow. For some typical propagation phenomenon, the discretisation grid (space and time) necessary for a complete representation is very heavy. We consider here an acoustic wave propagation based on the Euler equations.

In order to apply an unsteady mesh adaptation, we adopt the so-called Global-Fixed-Point (GFP) algorithm, [16]. In short, the time interval is divided in n_{adap} sub-intervals. After a computation of state and adjoint on the whole time interval, an optimal space-time metric is evaluated as a the n_{adap}-uple of optimal spatial metrics for each of the time sub-intervals.

In Figure 7, the propagation of a noise from a road (bottom left) to a balcony (near top, right) around an anti-noise wall (middle of bottom) is computed. The functional is the pressure integral on an interval of the balcony. Since a few wavelengths are emitted at the noise source, the mesh adaptation process will concentrate on the part of the wave train which will hit the balcony. This dramatically reduces the region of

the computational domain which needs to be refined. With 30980 vertices (mean of the 20 meshes used over the time interval) the error on the integral of pressure on the balcony is about 1%. The local resolution is about 10 points per half wave and a uniform mesh with same resolution would involve 5 millions vertices.

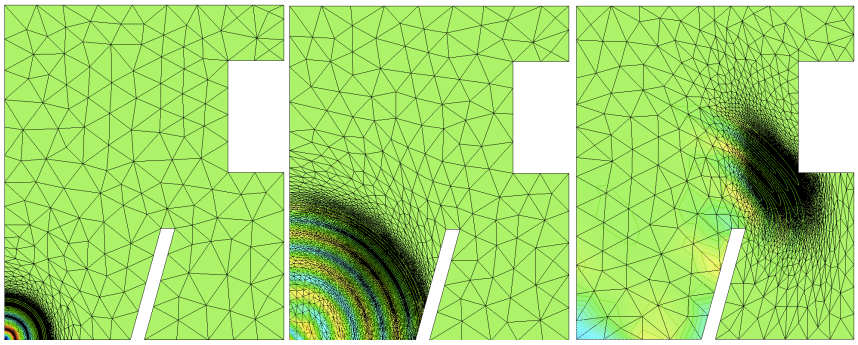

Fig. 7 Goal Oriented unsteady calculation of nonlinear acoustics propagation with third-order goal-oriented adaptation. Pressure at three different time levels and the corresponding meshes.

With this GFP algorithm, we have maximized the safety by always choosing meshes as fine as or finer than necessary. The GFP involves a delicate compromise between efficiency and accuracy. Indeed, if the number of meshes during the time-interval is low, then each mesh is adapted to the evolution of solution over a large interval and is therefore heavier than with a smaller time-interval and of course even still heavier than a mesh adapted to a precise time step. This disadvantage amplifies if a thin detail (a discontinuity for example) in the solution is traveling, since the mesh will be extremely refined over the whole region swept by the detail. Conversely, if many adapted meshes are used in the time-interval, then there will be many transfers from a previous mesh to the next one. Now these transfers have been identified as deteriorating the solution, in an extent which justifies to avoid hundreds transfers in a computation. A way to partly avoid this compromise may be to move the mesh. Then mesh admissibility would be accounted by local repairing at some instant. It is anticipated that these repairings would bring less inaccuracy that global mesh-to-mesh transfers.

4 A discussion of singularity capturing

The sign of a complete success for a mesh adaptive algorithm is that for singular cases the numerical convergence order α is as high as the numerical convergence order α_{scheme} on smooth cases, according to:

$$|u - u_N| \leq const.\, N^{\frac{\alpha}{dim}} \quad , \quad \alpha = \alpha_{scheme}$$

where N is the total number of nodes representing the approximate PDE solution and dim the computational dimension (space dimension for steady, space-time dimension for unsteady). Unfortunately, this convergence for singular cases faces many barriers related to the family of meshes considered in the adaptation step, rather independantly of the underlying approximation. Let us mention two important examples of such barriers. In the steady (2D/3D) case, mesh adaptation cannot converge at second-order on a discontinuity if it does not involve anisotropy in arbitrary direction. In the unsteady case (N being the total space-time nodes), convergence at second order is not obtained when time stepping uses a (spatially) uniform time step. For this second issue, some progress should be expected from multi-rate time stepping (see [24, 25]). The next two subsections concentrate on the high-order singularity capturing issue for steady calculations. The third one on unsteady case.

4.1 Low order interpolation error (1D)

When a second-order approximation is applied to a singular variable, the output generally show a more or less developed oscillatory zone close the the singularity. About one decade of research around the 80's produced TVD/LED schemes which are thought as fully second-order accurate far from the singularity and first-order near the singularity and non-oscillatory. This accuracy statement is true for local approximations like the interpolation of a given function. But the global error is at most of first order for example in L^1 norm (order zero in L^∞) for a series of uniform meshes. For the approximate solution of a PDE, this accuracy statement is also false: in many case it will be globally first-order accurate, in particular in L^1. It is interesting to analyse how the above FB, GO, NO mesh adaptation technologies behave in presence of a singularity (typically a discontinuity through a smooth surface in 3D).

To discuss the feature-based option we consider the basic problem of mesh-adaptive interpolation of a the sum of a quadratic function with a Heaviside 1D function $h(x) = 1/2(sign(x) + 1)$. The derivative of h at zero is a Dirac δ_0 and its Hessian is a δ_0'. Looking at the P_1 interpolation on a regular mesh, the absolute value of the Hessian is proportional to $1/\Delta x^2$ on the two points close to zero, that is on a support of $O(\Delta x$ width). After a short calculation of the optimal metric for L^1 interpolation, the optimal strategy divides by four the interval containing zero and by two the other ones, which produces a second-order accurate convergence. This illustrates that although the interpolation error analysis defining the Hessian term as a representative main term of the error is not rigorous, keeping this Hessian in the feature-based adaptation makes a reasonable job.

Let us mention that this analysis extends to the multi-dimensional context and to the goal/norm-oriented approach, and that second-order convergence also holds with curved singularity supports. Let us give an example (Figure 8). A typical problem in multiphase flow is the discontinuity of pressure gradient along an interface.

Our model problem is a Poisson problem with a discontinuous coefficient. We apply a uniform refinement, a feature-based adaptation and a norm-oriented mesh adaptation, converging them by increasing the number of vertices. With both mesh adaptive approaches, second-order convergence is obtained. In contrast, uniform mesh refinement produces a disastrous first-order convergence with still a 10% error when using a 300×300 mesh.

4.2 Higher order interpolation error

In the case of an approximation of order 3, like a quadratic central ENO scheme ([23]), a discontinuity has influence on a thick set of approximation molecules. Our 1D estimate involves a third-order finite difference, weighted by $1/\Delta x^3$ also with a support width of a few Δx. It is interesting to use limiters which return to first order through the discontinuity in order to show a *thin shock structure*, easier to capture with a small number of nodes.

Passing to multidimensional case, let us examine the configuration where the exact solution involves a discontinuity aligned with a rather regular surface. Geometrically, the discontinuity can be put between two lines(2D)/surfaces(3D) of nodes.. This results in a too large number of nodes if the mesh is isotropic, but a smaller number of nodes (allowing second-order convergence) if the mesh is with straight edges and anisotropic, and finally a reasonable number of nodes (allowing higher-order convergence) if the mesh is anisotropic and the edges are curved.

Due to $(k+1)$-th order accuracy far from the singularity, a sequence of mesh which divide by two the regular part of the mesh should divide by at least 2^{k+1} the elements crossed by the discontinuity where convergence accuracy is less or equal unity. Now, according to the type of high-order approximation, the numerical capturing will be spread over one or several high-order elements. Then a refinement region covering a time interval may cover several times 2^{k+1} elements. It may become fairly computational cost consuming. Again an evident way to reduce this cost is to use an approximation with one cell per element, like the above refered ENO scheme ([23]), and combine with a shock capturing mechanism which reduce locally the order to one and essentially limits the numerical shock to be spread between only two continguous lines(2D)/surfaces(3D) of cells.

This strategy is applied for obtaining a steady scram jet flow (Figure 9) with adaptive capturing of the shocks as thin (in terms of width and of cells) as possible. This test case does not involve curved discontinuities for which our adapted mesh with straight edges would face an accuracy barrier (accuracy limited to two). From this standpoint, the path for third-order mesh adaptation indeed involves the mastering of curved elements, see for example [29].

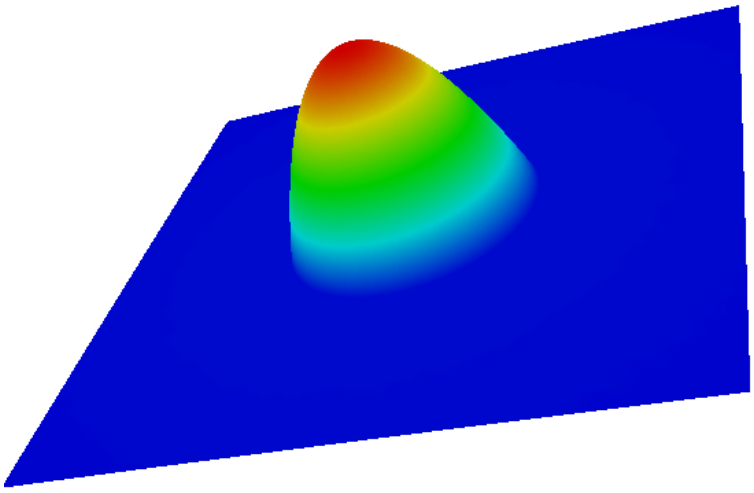

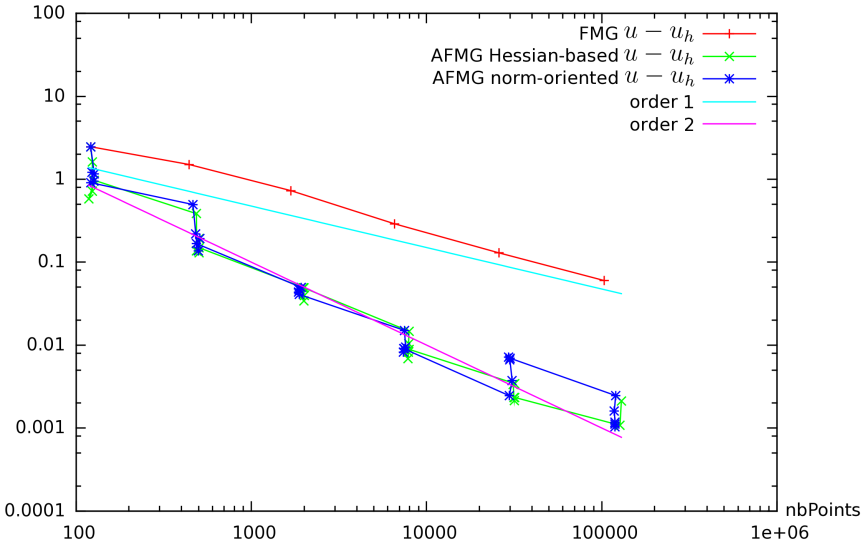

Fig. 8 Mesh-adaptive calculation of a pressure with discontinuous gradient due to an interface. The second order mesh convergence (in terms of number of vertices) of a feature-based adaptation and a norm-oriented adaptation are compared with the first-order uniform refinement.

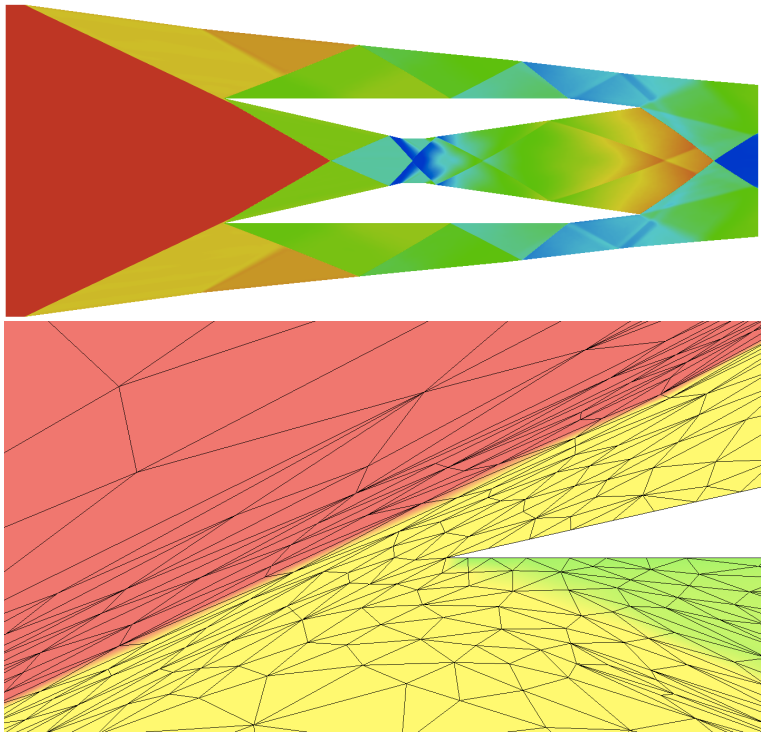

Fig. 9 Mesh-adaptive third-order accurate calculation of a scramjet flow, Mach contours, global view, and zoom around the bottom leading edge (improved palette).

4.3 Complexity analysis for the CENO-based Global Fixed Point

The space-wise third-order capture of the singularity can be addressed by spatial mesh adaptation: for each time level, we apply a metric-based anisotropic spatial mesh adaptation. Mesh size normal to the discontinuity will be reduced by a factor 8, *solely* in the vicinity of the discontinuity. In other directions near discontinuity and in any direction in other regions of the computational domain, the mesh size is divided by only 2. Then the increment in number of nodes near the discontinuity is asymptotically negligible and in the total, passing from N spatial degrees of freedom to $4N$ leads to a eight times reduction of the spatial error.

Unfortunately, the unsteady case is more difficult. In 2D, for decreasing accordingly time discretization error, the time step also needs to be reduced by a factor 8, leading to a total number of degrees of freedom multiplied by 32. Thus:

$$||u - u_{64N}||_{L^1(\Omega\times[0,T])} \leq \frac{1}{4}||u - u_N||_{L^1(\Omega\times[0,T])}\,. \tag{9}$$

By comparing $\frac{1}{4}$ with $32^{-\alpha/n}$, this time with $n=3$ (space-time dimension), we get a space time convergence order $\alpha = 8/5$.

In 3D, with this strategy, passing from N spatial degrees of freedom to $8N$ leads to a eight times reduction of the spatial error. Unfortunately, the time step also needs to be reduced by a factor 8, leading to a total number of degrees of freedom multiplied by 64. Thus:

$$||u-u_{64N}||_{L^1(\Omega\times[0,T])} \leq \frac{1}{4}||u-u_N||_{L^1(\Omega\times[0,T])}. \tag{10}$$

By comparing $\frac{1}{4}$ with $64^{-\alpha/n}$, this time with $n=4$ (space-time dimension), we get $\alpha = 4/3$ which is even smaller.

Lemma: *(Barrier of convergence order for time stepping CENO3 discretization) for a time-stepping third-order flow solver coupled with an unsteady goal-oriented mesh adaptation at each time level applied to a traveling discontinuity, the space-time convergence rate is at most* $\alpha = 8/5$ *for 2D unsteady calculations and and* $\alpha = 4/3$ *for 3D unsteady calculations.*

This analysis extends to our Global Fixed Point if the number of time steps is kept constant while the adapted mesh is frozen. In other words, in 3D for example, when we pass from N space-time nodes to $64N$, the number of meshes over the time interval must be multiplied by 8, which may fastly amplify the mesh-to-mesh transfer error.

As already mentioned, this barrier can be overcome with a full space-time adaptive time stepping (with space-time elements) or by applying a multirate strategy.

5 Conclusions

This review of recent progress in mesh adaptation has validated the many promises made by this numerical technology. The promises concern the calculation of new complex (singular/multi-scale, coupled) phenomenas in continuum mechanics, which were not affordable before. This is conditioned by the design of algorithms which show a *numerical convergence for non-regular phenomenas* (in terms of number of nodes used) really better than shown by existing ones. For this purpose, we are increasing our knowledge of the conditions under which mesh adaptive steady high-order methods will enjoy high numerical convergence order.

Simultaneously, correctors are derived in order to improve our control on error level.

Clearly, for steady calculations, things are progressing rather fastly. The optimal order of convergence can be obtained and this results in the success of computations, like sonic boom, which were not possible without automatic mesh adaptation. But the highest expectation concerns *unsteady phenomena*. Some preliminary successes show that much can be expected in this direction. At the same time, many difficulties

remain to be solved before unsteady mesh adaptation methods show the maximal numerical convergence order.

The roadmap for being able to compute new phenomenas includes of course the further development of *efficient unstructured higher-order approximations*. This issue, not discussed here, is progressing (see an interesting discussion in [30]).

Once the number of nodes for the expected accuracy is made small, it remains to reduce the number of arithmetic operations to solve the discrete PDE system. Novel *solution algorithms* should be combined with the mesh-adaptation loop in order to produce the most performing global mesh-adaptation/system resolution algorithms. Algorithms combining $O(N)$ complexity and parallel scalability are compulsory. Also, the iterative PDE solver should be a good *corrective* solver, that is a solver which leads efficiently from a rather good initial field to a better/just as necessary converged solution field. The steady case is again an easier case and we refer to [31] for a FMG-adaptive proposal.

6 Acknowledgements

Alain Dervieux's thesis was advised by Roland Glowinski. Happy birthday Roland and many thanks.
This work has been supported by French National Research Agency (ANR) through project MAIDESC n^o ANR-13-MONU-0010. This work was granted access to the HPC resources of CINES under the allocations 2017-A0022A05067 and 2017-A0022A06386 made by GENCI (Grand Equipement National de Calcul Intensif).

References

1. Alauzet, F., & Loseille, A., 2010. High order sonic boom modeling by adaptive methods. *J. Comp. Phys.*, 229:561–593.
2. Loseille, A., & Löhner, R., 2010. Adaptive anisotropic simulations in aerodynamics. In *48th AIAA Aerospace Sciences Meeting and Exhibit*, AIAA-2010-169, Orlando, FL, USA.
3. Loseille, A., & Löhner, R., 2011. Boundary layer mesh generation and adaptivity. In *49th AIAA Aerospace Sciences Meeting and Exhibit*, AIAA-2011-894, Orlando, FL, USA.
4. Castro-Díaz, M.J., Hecht, F., Mohammadi, B., & Pironneau, O., 1997. Anisotropic unstructured mesh adaptation for flow simulations. *Int. J. Num. Meth. in Fluids*, 25:475–491.
5. Dompierre, J., Vallet, M.G., Fortin, M., Bourgault, Y., & Habashi,W.G., 1997. Anisotropic mesh adaptation: towards a solver and user independent CFD. In *AIAA 35th Aerospace Sciences Meeting and Exhibit*, AIAA-1997-0861, Reno, NV, USA, Jan 1997.
6. Vasilevski, Y.V., & Lipnikov, K.N., 2005. Error bounds for controllable adaptive algorithms based on a hessian recovery. *Computational Mathematics and Mathematical Physics*, 45(8):1374–1384, 2005.
7. Huang, W., 2005. Metric tensors for anisotropic mesh generation. *J. Comp. Phys.*, 204:633-665, 2005.
8. Frey, P.J., & Alauzet, F., 2005. Anisotropic mesh adaptation for CFD computations. *Comp. Meth. Applied Mech. Eng.*, 194(48-49):5068–5082.

9. Chen, L., Sun, P., & Xu, J. 2007. Optimal anisotropic meshes for minimizing interpolation errors in L^p-norm. *Math. Comp.*, 76(257):179-204, 2007.
10. Loseille, A., & Alauzet, F., 2011. Continuous mesh framework. Part I: well-posed continuous interpolation error. *SIAM NUMA*, 49:1,38-60.
11. Loseille, A., & Alauzet, F., 2011. Continuous mesh framework. Part II: validations and applications. *SIAM Num. Anal.*, 49(1):61–86.
12. Becker, R., & Rannacher, R. 1996. A feed-back approach to error control in finite element methods: basic analysis and examples. *East-West J. Numer. Math.*, **4**, 237–264.
13. Brèthe, G., & Dervieux, A. 2016. Anisotropic Norm-Oriented Mesh Adaptation for a Poisson problem. *J. Comp. Phys.*, 322, 804 826.
14. Loseille, A., Dervieux, A., & Alauzet, F. 2015. Anisotropic Norm-Oriented Mesh Adaptation for Compressible Flows. *In: 53rd AIAA Aerospace Sciences Meeting*. AIAA-2015-2037, Kissimmee, Florida.
15. Loseille, A., Dervieux, A., Frey, P.J., & Alauzet, F. 2007. Achievement of global second-order mesh convergence for discontinuous flows with adapted unstructured meshes. *In: 37th AIAA Fluid Dynamics Conference and Exhibit*. AIAA-2007-4186, Miami, FL, USA.
16. Belme, A., Dervieux, A., & Alauzet, F. 2012. Time Accurate Anisotropic Goal-Oriented Mesh Adaptation for Unsteady Flows. *J. Comp. Phys.*, 231:19, 63236348
17. Pierce, N. A. and Giles, M. B., 2000. Adjoint Recovery of Superconvergent Functionals from PDE Approximations, *SIAM Review*, 42:2, 247-264.
18. Yano, M., & Darmofal, D., 2012. An optimization framework for anisotropic simplex mesh adaptation: application to aerodynamics flows. *AIAA Paper*, 2012-0079.
19. Ferro, N., Micheletti, S., & Perotto, S., 2018 Anisotropic mesh adaptation for crack propagation induced by a thermal shock in 2D. Accepted for the publication in *Comput. Methods Appl. Mech. Engrg.*.
20. Formaggia, L., & Perotto, S., 2003. Anisotropic a priori error estimates for elliptic problems. *Numer. Math*, 94:67-92.
21. Barth, T.J., & Frederickson, P.O., 1990. Higher order solution of the Euler equations on unstructured grids using quadratic reconstruction, AIAA Paper 90-13.
22. Ivan, L., & Groth,C.P.T., 2014. High-order solution-adaptive central essentially non-oscillatory (CENO) method for viscous flows. *J. Comp. Phys.*, 257:830-862.
23. Carabias, A., Belme, A., Loseille, A., & Dervieux, A., 2017. Anisotropic goal-oriented error analysis for a third-order accurate CENO Euler discretization. *Int. J. Num. Meth. in Fluids*, http://dx.doi.org/10.1002/fld.4423
24. Seny, B., Lambrechts, J., Toulorge, T., Legat, V., & Remacle, J.-F., 2014. An efficient parallel implementation of explicit multirate Runge-Kutta schemes for discontinuous Galerkin computations. *J. of Comp. Phys.*, 256:135–160.
25. Itam, E., Wornom, S., Koobus, B., & Dervieux, A., 2016. A Volume-Agglomeration Multirate Time Advancing Approach. ECCOMAS Congress 2016 VII European Congress on Computational Methods in Applied Sciences and Engineering, Hernissios, Crete, Greece. hal-01413449
26. Coulaud, O., & Loseille,A., 2016. Very High Order Anisotropic Metric-Based Mesh Adaptation in 3D. 25th International Meshing Roundtable. *Procedia Engineering*, 163, 353-365.
27. Frazza, L., Loseille, A., Alauzet, F. & Dervieux, A., 2018. Nonlinear corrector for RANS equations, AIAA conf. 2018.
28. Coupez, T., 2011. Metric construction by length distribution tensor and edge based error for anisotropic adaptive meshing. *J. Comp. Phys.*,230, 2391-2405.
29. Dobrzynski, C. & El Jannoun, G., 2017. High order mesh untangling for complex curved geometries. INRIA RR-9120.
30. Vincent, P.E., & Jameson, A., 2011. Facilitating the adoption of unstructured high-order methods amongst a wider community of fluid dynamicists, *Math. Model. Nat. Phenom.*, 6:3,97-140.
31. Brethes, G., Allain, O., & Dervieux, A., 2015. A mesh-adaptative metric-based full multigrid for the Poisson problem, *Int. J. Num. Meth. in Fluids*,79-1, 3053.
32. 2nd AIAA Sonic Boom Prediction Workshop (2017) Grapevine, Texas.